

Patterns without patches: Hierarchical assembly of complex structures from simple building blocks

Michael Grünwald

Computational Physics, University of Vienna, Sensengasse 8, 1090 Vienna, Austria

Phillip L. Geissler

Department of Chemistry, University of California, Berkeley, California 94720

Nanoparticles with "sticky patches" have long been proposed as building blocks for the self-assembly of complex structures. The synthetic realizability of such patchy particles, however, greatly lags behind predictions of patterns they could form. Using computer simulations, we show that structures of the same genre can be obtained from a solution of simple isotropic spheres, provided control only over their sizes and a small number of binding affinities. In a first step, finite clusters of well-defined structure and composition emerge from natural dynamics with high yield. In effect a kind of patchy particle, these clusters can further assemble into a variety of complex superstructures, including filamentous networks, ordered sheets, and highly porous crystals.

Living systems create and maintain their functional microscopic organization through self-assembly, the spontaneous arrangement of an initially unordered collection of biomolecular building blocks. Mimicking this behavior in the laboratory with synthetic components has proven to be a formidable challenge. A close look at the agents of self-assembly in living systems reveals a key aspect of the problem: Most biomolecular objects interact through directionally specific forces, so-called "patchy" interactions. Indeed, computer simulations of model nanoparticles with attractive patches have recapitulated much of the richness of nature's self-assembled structures [1–5]. Synthetic nanoparticles with controlled patchiness, however, are largely unavailable in the laboratory, although impressive progress has been made in specific cases [6–8].

In this letter, we consider a pragmatic question, though from a theoretical perspective: Using only nanoparticle synthesis and functionalization techniques that are standard today, can self-assembled patterns be realized that share the complexity achieved by biology's (and simulators') patchy components? In particular, we devise and demonstrate numerically a hierarchical strategy for this purpose, which assumes control only over a few energies of interaction between spherical particles, as well as their size. Such control should be feasible in practice given well-established procedures to decorate the exterior of nanoparticles with double-stranded DNA.

Our scheme begins with a dilute solution of spherical particles, of several types, that interact isotropically and over short distances. With appropriate choice of the sizes and binding affinities of these particles, we show that a nearly uniform population of "metaparticles" can emerge – tightly bound clusters, comprising a handful of spherical monomers, with defined composition and internal structure, as illustrated in Figure 1a. These objects constitute a kind of patchy nanoparticle, with nontrivial shape and an anisotropic arrangement of monomers

that can subsequently serve as sites for effectively directional interaction. In the second stage of our scheme, the emergent patchiness of metaparticles is exploited to spontaneously generate large-scale superstructures, some of which are highly ordered and reminiscent of biological assemblies.

The types of spherical monomers we have in mind are distinguished from one another by the strength of their interactions with other monomers. Specifically, the potential energy of two monomers, of types A and B , separated by a distance r is $u_{\text{rep}}(r) + \epsilon_{AB}u_{\text{att}}(r)$. The steric repulsion u_{rep} enforces volume exclusion, strongly penalizing separations below a threshold value, $r \leq \sigma$. At distances near contact, the attractive potential u_{att} provides a favorable energy, $u_{\text{att}}(r) \approx -1$ for $r \leq \sigma + w$, and attenuates rapidly for $r > \sigma + w$.

The specific forms of these potentials are not important, only that u_{rep} sets a well-defined particle diameter σ and that u_{att} acts over a short range $w \ll \sigma$ [28]. Colloidal nanoparticles with surface-grafted DNA molecules provide one experimental realization of this system, in which the complementary sequences of DNA strands attached to monomers A and B encode the strength ϵ_{AB} of their attraction [9–11].

Building finite-sized metaparticles from a macroscopic collection of such monomers is not a trivial matter [12–14]. If, say, attractions among monomers A , B , C , and D provide the cohesive energy maintaining the integrity of an $ABCD$ cluster, then additional monomers of these four types will tend to bind at the cluster's surface. Lacking constraints on monomer valency, it is not clear how to design against unbounded growth of a close-packed crystal.

Indeed, an extensive search through possible combinations of binding affinities did not yield self-limiting growth of small clusters in computer simulations.

To prepare metaparticles we instead adapted an approach devised to build finite clusters of identical par-

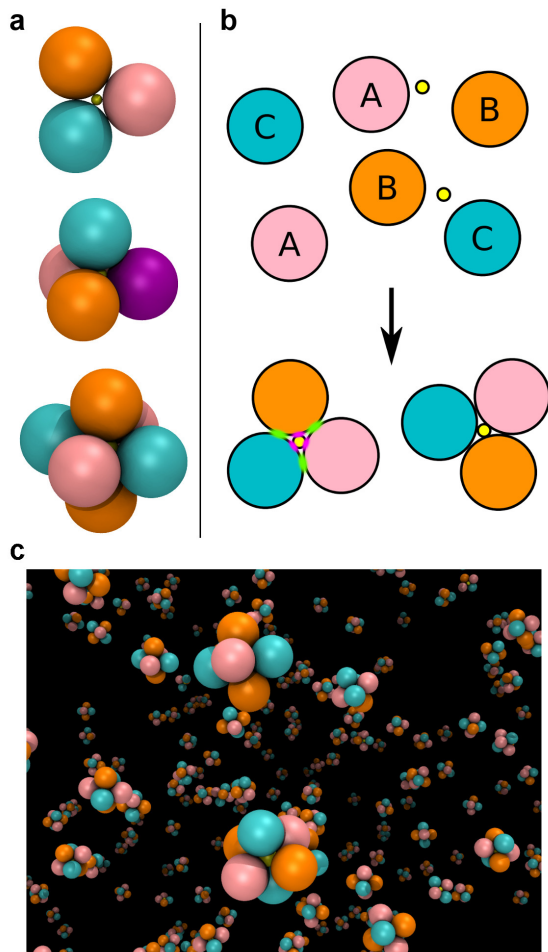


FIG. 1: **Self-assembly of metaparticles.** (a) Three example metaparticles that can be prepared with high yield through appropriate choices of attraction strengths and glue particle size. (b) Strategy for controlling cluster size and composition. Purple contact points indicate strong attraction between glue particles (yellow) and monomers [pink (A), orange (B), and blue (C)], which dictates metaparticle size and shape. Composition and connectivity within a metaparticle are controlled through weaker interactions (green contact points) between monomers. In this example, all unlike particle types attract one another; like types do not. (c) Snapshot from a simulation of C_6 metaparticle formation (with $\bar{\epsilon} = 3 k_B T$ and $\epsilon_{\text{glue}} = 10 k_B T$), after equilibrium has been established. For clarity we show only monomers that are bound to glue particles. The yield of correctly composed octahedral metaparticles in this case is $\approx 90\%$.

ticles [15, 16]. Here, cluster size and geometry are dictated by introducing an additional kind of particle with smaller diameter $\sigma_{\text{glue}} < \sigma$. This “glue particle” attracts all other monomers strongly (with contact energy ϵ_{glue}) and over short range (w_{glue}). For appropriate size combinations, the propensity to maximally coordinate each glue particle determines with great precision the structure of its shell of monomers, as illustrated in Figure 1b. Of the many convex polyhedra that can be obtained in

this way (denoted C_n , where n is the number of shell particles), we focus exclusively on triangles (C_3), tetrahedra (C_4), and octahedra (C_6) illustrated in Figure 1a. Unlike larger shapes, we can control the arrangement of monomer types within these shells through the set of attraction strengths $\epsilon \equiv \{\epsilon_{AA}, \epsilon_{AB}, \dots\}$, as discussed below.

The only threat to self-limiting growth in this scenario is the possibility that two glue particles bind to overlapping sets of shell monomers. This errant growth can be made irrelevant by working at low concentration of glue particles. Alternatively, they could be endowed with longer-range repulsions. Our simulations follow the latter approach, with glue particles repelling one another through a screened Coulomb interaction (see Methods).

The crux of making well-defined metaparticles lies in dictating the identities of monomers at each vertex of the shell. Out of the many possible shell compositions, illustrated for C_4 clusters in Supplementary Figure 1, one must be represented with dominant statistical weight. As one challenge to this task, ϵ_{glue} must be sufficiently weak that binding is reversible, so that inevitable mistakes in cluster composition can be corrected in reasonable time; cluster integrity may be compromised as a result. More subtly, attractions among shell particles must be sufficiently weak that they do not macroscopically condense. This constraint limits the extent to which one shell composition can dominate energetically over others. It is not obvious that these competing requirements can all be satisfied with a single choice of ϵ_{glue} and ϵ .

Approximate analytical calculations, as well as explicit Brownian dynamics simulations, indicate that high yields of certain metaparticles can in fact be made in this simple fashion (see Supplementary Methods and Supplementary Figure 2). As a straightforward design, we set $\epsilon_{ij} = \bar{\epsilon}$ if monomer types i and j make contact in a desired cluster, and $\epsilon_{ij} = 0$ otherwise [17]. Due to the limitations of short-ranged, pairwise, and isotropic interactions, this scheme does not permit access to all metaparticle compositions. For example, we cannot generate a pure population of octahedra with more than three monomer types. However, the metaparticles shown in Figure 1a can be prepared with high fidelity through spontaneous dynamics of initially dispersed monomers and glue particles. (See Figure 1b; simulation details are given in the Methods section.) In particular, we achieve maximum yields of 94%, 78%, and 98% for C_3 , C_4 , and C_6 clusters respectively. In the assembly of C_4 clusters, the two enantiomers of an $ABCD$ tetrahedron must appear with macroscopically identical concentrations – in simulations of superstructure assembly described below we consider the racemic mixture. In all cases, the emergent patchiness of clusters is sufficient to generate a rich variety of self-assembled superstructures.

To induce further assembly among many metaparticles, it is necessary at this point to modify the strengths

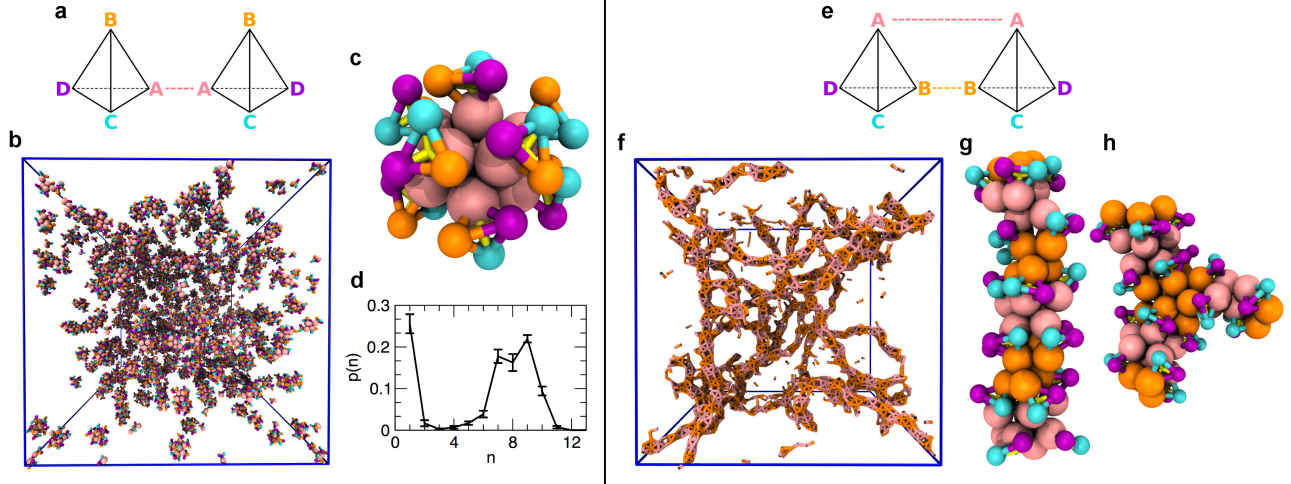


FIG. 2: **Zero- and one-dimensional assemblies** (Left) Micelle-like superstructures. Attractions of type $[AA]$ (indicated by the dashed pink line in (a)) between C_4 metaparticles yield self-limiting growth of superclusters whose interiors are dense in A monomers. (b) Snapshot from a molecular dynamics simulation, showing a dispersed collection of micelles. (c) An example micelle comprising 9 C_4 clusters. (d) Normalized histogram of the number of metaparticles within each micelle. (Right) Filamentous assemblies. Attractions of type $[AA, BB]$ (indicated by the dashed pink and orange lines in (e)) between C_4 metaparticles yield percolating networks of branched filaments. (f) Snapshot from simulation, showing only $A-A$ and $B-B$ bonds. An example filament segment (g) and branch point (h). The filament core consists of alternating A -rich and B -rich regions; non-attracting monomers of type C and D form a loose shell around the core. (In panels (b), (c), (g), and (h) non-attracting monomers are shown in smaller size for clarity.)

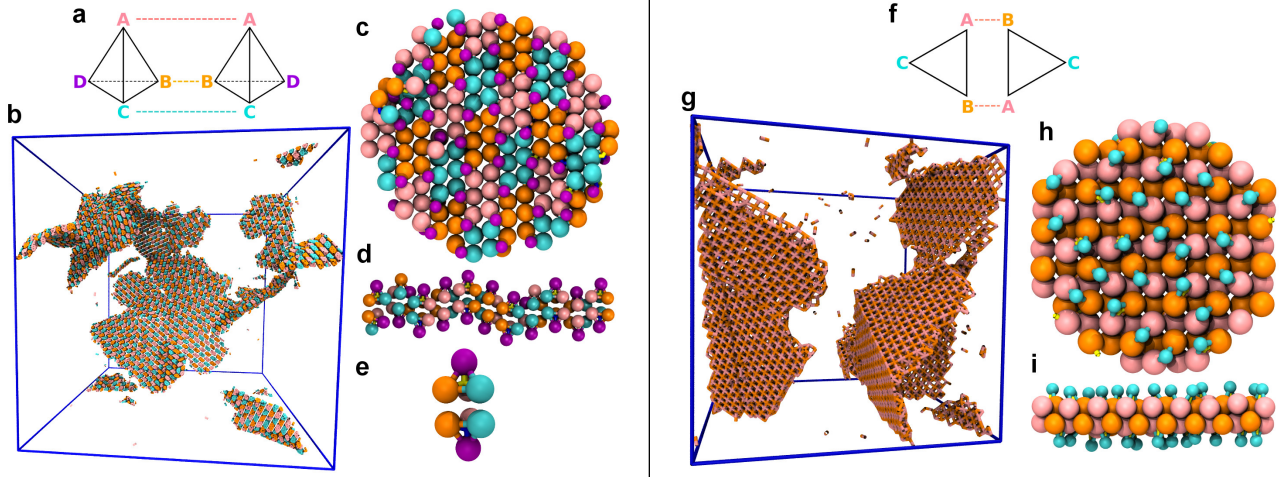


FIG. 3: **Two-dimensional assemblies** (Left) Bilayer sheets of C_4 metaparticles. Attractions of type $[AA, BB, CC]$ (indicated by the dashed pink, orange, and blue lines in (a)) yield sheets two metaparticles thick. (b) Snapshot from a molecular dynamics simulation, showing a collection of sheets linked at grain boundaries. (Only $A-A$, $B-B$, and $C-C$ bonds are shown.) (c) Top view of an example sheet, whose attracting monomers are arranged in groups of 12 in a regular pattern. Metaparticles with different chirality alternate in the sheet plane. (d) Side view of the same example sheet, highlighting its corrugation. (Centers of enantiomers are shown yellow and blue.) (e) Each cluster is bound to its mirror image in the opposite layer of the sheet. (Right) Bilayer sheets of C_3 metaparticles. Attractions of type $[AB]$ (indicated by the dashed lines in (f)) yield sheets that are flat and highly ordered. (g) Snapshot from a molecular dynamics simulation, showing only the bonds between A and B monomers. Of the two disconnected sheets, one exhibits extended kink defects. Top (h) and side views (i) of an example sheet highlight the face-centered-cubic-like bonding geometry. (In panels (c)–(e), (h), and (i) monomers are shown in smaller size for clarity.)

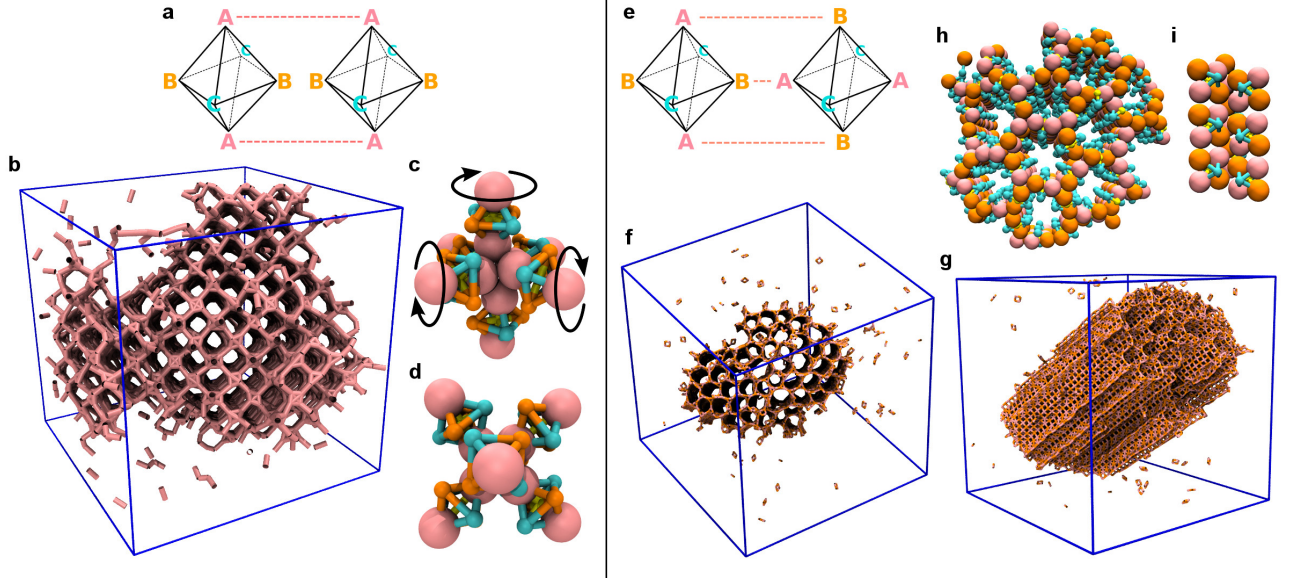


FIG. 4: **Three-dimensional assemblies.** (Left) A rotator phase with cubic symmetry. Attractions of type $[AA]$ (indicated by the dashed pink lines in (a)) between C_6 metaparticles yield a cage-like supercrystal. (b) Snapshot from a molecular dynamics simulation, showing only the bonds between A monomers. ((c) and (d)) An example vertex of the superlattice viewed from two different perspectives. Each vertex involves six C_6 clusters, bound through A - A attractions in a cross-like geometry. Metaparticle centers occupy the Wyckoff $3d$ positions of a cubic crystal with space group 221 ($Pm\bar{3}m$). The maximal packing fraction of the crystal is ≈ 0.42 . Each metaparticle can rotate freely around its A - A axis, as indicated by arrows. (Right) Honeycomb supercrystal. Attractions of type $[AB]$ (indicated by the dashed pink lines in (e)) between C_6 metaparticles yield a superstructure featuring extended channels arranged in a hexagonal pattern. ((f) and (g)) Simulation snapshot, showing only the bonds between A and B monomers, viewed from two different perspectives. ((h) and (i)) Excerpts from the honeycomb viewed along the channel axis and from its side. Channels are defined by circular arrangements of six C_6 clusters; non-attracting particles of type C point towards the center of the pore. (In panels (c), (d), (h), and (i) non-attracting monomers are shown in smaller size for clarity.)

of attraction ϵ between their constituent monomers, which now act as sticky patches for interactions between distinct clusters. To avoid consequent changes in metaparticles' internal structure, it is further necessary to render the glue particle bonds irreversible. Both of these tasks have been accomplished in other contexts using techniques of DNA nanotechnology [11]. Fortunately, elaborate combinations of monomer attraction are not needed at this stage to assemble complex patterns. On the contrary, introducing substantial attractions between more than one or two monomer types typically allows only close-packed crystals or amorphous solids as products of assembly. We have instead obtained interesting and varied assembly when $\epsilon_{ij} = 0$ for all monomer-monomer interactions except: (i) self-attraction of one monomer type, i.e., $\epsilon_{AA} > 0$ (a design we denote $[AA]$); or (ii) self-attraction of two types, $\epsilon_{AA} > 0$ and $\epsilon_{BB} > 0$ (denoted $[AA, BB]$); or (iii) a single cross-interaction, $\epsilon_{AB} > 0$ (denoted $[AB]$). In one special case the design $[AA, BB, CC]$ was also conducive to nontrivial pattern formation. As is generally the case with patchy nanoparticles, the dynamical fate of assembly is very sensitive to the magnitudes of these attractions [18–20]. We explored a range of values of ϵ_{AA} , ϵ_{BB} , etc. for each struc-

ture and report here on choices that yielded the most reproducible and defect-free assemblies. For an attraction range $w \approx 0.05\sigma$, well depths of a few $k_B T$ appear to be optimal in all cases (see Methods). For some designs the energetic range between impractically slow growth and extensively defective aggregation is as narrow as $0.2 k_B T$. The superstructures described below were assembled from metaparticles of uniform composition; their quality was only slightly degraded by including defective metaparticles at the levels indicated by simulations of cluster formation.

Given that metaparticle structures are highly symmetric, and that the size of effective patches is prescribed by the monomer diameter, one might expect the variety of patterns that can be assembled from the C_3 , C_4 , and C_6 clusters of Figure 1a to be meager and easily anticipated. These objects, however, are more complex building blocks than spheres decorated with symmetric interaction sites. Indeed, particle shape can be a critical factor in self-assembly, strongly influencing the structure of thermodynamic ground states as well as their kinetic accessibility[21–23].

An interplay between packing and directional attraction is important in even the simplest assembly we ob-

served in Brownian dynamics simulations of interacting metaparticles. (Simulation details are given in the Methods section.) With only one mode of self-attraction ($[AA]$) among monomers in different C_4 clusters, the attracting species A tends to aggregate to the extent allowed by volume exclusion due to the rest of the cluster. Zero-dimensional, micelle-like superstructures thus naturally emerge (see Figure 2a), and like conventional micelles they are not uniform in size. Because of metaparticles' anisotropic shape, the average size and polydispersity of these superstructures are the result of a complicated competition between the energetic drive to expand the A -rich cores and the entropic cost of packing (bumpy) tetrahedra at locally high density.

Adding a second self-attraction to C_4 species ($[AA, BB]$) effectively encourages aggregation within and among the micellar superstructures just described. Due to constraints of packing and stoichiometry, B monomers on the micelle exterior segregate to opposite poles, where they can bind to the poles of other micelles. This linear motif may extend indefinitely, generating one-dimensional super-filaments with an internal pattern of alternating A -rich and B -rich cores, as shown in Figure 2b. The fluctuations responsible for micelle size variation in the $[AA]$ case here produce local defects in core thickness and exposure. Some of these defects cause sufficient exposure of the cylindrical core to allow filament branching. At high metaparticle density, percolating networks of filaments reminiscent of biopolymer gels result [24].

Adding a third attraction to this scenario ($[AA, BB, CC]$) once again increases the dimensionality of assembled superstructures. Only monomers of type D are inert in this case, and they can be sequestered to the opposing faces of an ordered sheet that is two metaparticles thick, as illustrated in Figure 3a. In its ideal form this superstructure features macroscopic lines of isochiral clusters, alternating with lines of their enantiomers. Such chiral micropatterning might provide a basis for engineering unusual optical properties. Sheets forming on the time scale of our simulations possess a significant number of defects that define grain boundaries between domains of different orientation.

Triangular metaparticles were similarly observed to form sheets (with $[AB]$ and $[AA, BB]$ attractions) and micelles (with $[AA]$ attractions), as illustrated in Figure 3b and Supplementary Figure 3. Octahedral clusters, on the other hand, generate exotic three-dimensional superlattices. In one such crystal ($[AA]$), C_6 metaparticles maintain complete rotational freedom about the axis connecting attractive monomers (see Figure 4a). Another crystal (obtained with $[AB]$ and $[AA, BB]$) is highly porous, with a packing fraction of ≈ 0.12 , and is traversed by hexagonal channels (see Figure 4b and Supplementary Figure 4). Both offer intriguing design possibilities for molecular adsorption and metamaterials.

While this survey of assemblies is not necessarily ex-

haustive, we believe it to be thorough for metaparticles accessible with high yield through the procedures we have described. Mixtures of metaparticles with varying composition are in fact easier to prepare, at least in the proportions dictated by their thermodynamic stabilities. Such mixtures expand the range of superstructures that can be achieved through our hierarchical protocol. As one example, C_6 clusters of uniform composition $ABCBCD$ cannot be prepared with high yield from our strategy. However, a mixture of $ABCBCD$, $ABCBCA$, and $DBCBCD$ clusters (in average proportions 2:1:1) can be straightforwardly generated, specifically by adding a fourth monomer type D to the collection of monomers that would otherwise form pure $ABCBCA$ clusters. In simulations, this mixture assembles into yet another distinct porous supercrystal, shown in Supplementary Figure 5. Many more such scenarios are possible and, more importantly, should be straightforward to realize using existing synthetic technologies.

Methods

Pair potential

The repulsive and attractive interaction potentials used in our simulations have the specific forms

$$u_{\text{rep}}(r) = \begin{cases} k_B T [1 + 4(\tilde{r}^{-12} - \tilde{r}^{-6})], & r < \sigma \\ 0, & r \geq \sigma, \end{cases}$$

where

$$\tilde{r}(r) = \frac{r - \sigma}{\alpha_{\text{rep}}} + 2^{1/6},$$

and

$$u_{\text{att}}(r) = \begin{cases} \frac{1}{2} \left[\tanh\left(\frac{r - (\sigma + w)}{\alpha_{\text{att}}}\right) - \tanh\left(\frac{w}{\alpha_{\text{att}}}\right) \right], & r < \sigma + 2w \\ 0, & r \geq \sigma + 2w. \end{cases}$$

The repulsive part, a shifted Lennard-Jones potential whose steepness is set by the length scale α_{rep} , vanishes continuously at $r = \sigma$. The attractive part, a well of approximately unit depth whose steepness near $r = \sigma + w$ is set by the length scale α_{att} , vanishes continuously at $r = \sigma + 2w$. Examples of the total interaction potential are plotted in Supplementary Figure 6. The standard mixing rule $\sigma = (\sigma_1 + \sigma_2)/2$ was used to determine interactions between particles with different diameters σ_1 and σ_2 .

Simulations

In all simulations we adopt $k_B T$ as a unit of energy, monomer diameter σ as a unit of length, monomer mass

m as a unit of mass, and $\tau = \sqrt{m\sigma^2/k_{\text{B}}T}$ as a unit of time. Our systems are then specified by the following dimensionless parameters: (a) glue particle diameter, $\sigma_{\text{glue}}/\sigma$, which we set to $\sqrt{4/3}-1$, $\sqrt{3/2}-1$, and $\sqrt{2}-1$, for C_3 , C_4 , and C_6 clusters, respectively; (b) glue particle mass, $m_{\text{glue}}/m = (\sigma_{\text{glue}}/\sigma)^3$, proportional to its volume; (c) monomer friction coefficient $\gamma\tau/m = 10$; and (d) glue particle friction coefficient $\gamma_{\text{glue}}\tau/m = 10\sigma_{\text{glue}}/\sigma$, proportional to its diameter. Dynamics were advanced by numerically integrating the underdamped Langevin equation, as implemented in the HOOMD-blue simulation package [25].

Cluster assembly

For simulations of metaparticle formation, we set $w = 0.035\sigma$, $\alpha_{\text{rep}} = 0.2\sigma$, and $\alpha_{\text{att}} = 0.01\sigma$. Initial conditions were constructed by randomly placing 500 glue particles and 1000 monomers (2000 in the case of C_6 clusters) of each type in a periodically replicated cubic simulation box at packing fraction 0.005. Trajectories of length $10^4\tau$ were generated with an integration time step $\Delta t = 10^{-4}\tau$. Binding of monomers to multiple glue particles was suppressed by a pairwise repulsion $u_{\text{glue-glue}}(r) = 40k_{\text{B}}T e^{-r/\sigma}(r/\sigma)^{-1}$. We calculate assembly yields as N_{t}/N , where N_{t} is the number of clusters with desired composition and N is the total number of clusters with the maximum number of monomers. Clusters that are not fully assembled are disregarded, as their population can be made negligible by an appropriate choice of ϵ_{glue} . Maximum yields were achieved with $\epsilon_{\text{glue}} = 10k_{\text{B}}T$ and $\bar{\epsilon} = 4k_{\text{B}}T$ for C_4 and C_6 metaparticles, and $\bar{\epsilon} = 4.4k_{\text{B}}T$ for C_3 clusters.

Superstructure assembly

Simulations of the second stage of assembly included 1000 to 8000 metaparticles, initially placed on a simple cubic lattice at densities between $0.04\sigma^{-3}$ and $0.01\sigma^{-3}$. Metaparticles were treated as rigid bodies [26]. Monomer interaction parameters were set as $w = 0.075\sigma$, $\alpha_{\text{rep}} = 0.3\sigma$, and $\alpha_{\text{att}} = 0.02\sigma$ (which allow use of a larger integration time step $\Delta t = 0.005\tau$). Glue particle repulsions were omitted at this stage. Time was advanced in each assembly trajectory by $5 \times 10^5\tau$.

The following attraction strengths resulted in the structures depicted in Figures 2, 3, and 4:

- C_4 micelles: $\epsilon_{\text{AA}} = 5.8k_{\text{B}}T$
- C_4 filaments: $\epsilon_{\text{AA}} = \epsilon_{\text{BB}} = 4.5k_{\text{B}}T$
- C_4 sheets: $\epsilon_{\text{AA}} = \epsilon_{\text{BB}} = \epsilon_{\text{CC}} = 3.7k_{\text{B}}T$
- C_3 sheets: $\epsilon_{\text{AB}} = 3.7k_{\text{B}}T$

- C_6 cubic rotator phase: $\epsilon_{\text{AA}} = 4.7k_{\text{B}}T$
- C_6 hexagonal channels: $\epsilon_{\text{AB}} = 4.15k_{\text{B}}T$

These values resulted in structures of the highest quality in our simulations. We note, however, that different values are likely to be optimal for different choices of pair potential (in particular, for a different range w of attraction, as discussed in Supplementary Methods), and for assembly trajectories that are substantially longer than the time scales accessible with current hardware.

Images of clusters and assemblies were rendered with VMD [27].

Acknowledgments

We thank Michael Brenner, Todd Gingrich, Sharon Glotzer, and Patrick Varilly for useful discussions. This work was supported by the Austrian Science Fund (FWF) under Grant J 3106-N16. Calculations were in part performed on the Vienna Scientific Cluster (VSC).

-
- [1] Zhang, Z., Keys, A., Chen, T. & Glotzer, S. Self-assembly of patchy particles into diamond structures through molecular mimicry. *Langmuir* **21**, 409–413 (2005).
 - [2] Vissers, T., Preisler, Z., Smalenburg, F., Dijkstra, M. & Sciortino, F. Predicting crystals of Janus colloids. *J. Chem. Phys.* **138**, 164505 (2013).
 - [3] Bianchi, E., Blaak, R. & Likos, C. N. Patchy colloids: state of the art and perspectives. *Phys. Chem. Chem. Phys.* **13**, 6397–410 (2011).
 - [4] Hagan, M. F. Modeling Viral Capsid Assembly. *arXiv preprint arXiv:1301.1657* 42 (2013). 1301.1657.
 - [5] Ouldridge, T. E., Louis, A. a. & Doye, J. P. K. Structural, mechanical, and thermodynamic properties of a coarse-grained DNA model. *J. Chem. Phys.* **134**, 085101 (2011).
 - [6] Wang, Y. *et al.* Colloids with valence and specific directional bonding. *Nature* **491**, 51–5 (2012).
 - [7] Chen, Q., Bae, S. C. & Granick, S. Directed self-assembly of a colloidal kagome lattice. *Nature* **469**, 381–4 (2011).
 - [8] Pawar, A. B. & Kretzschmar, I. Fabrication, assembly, and application of patchy particles. *Macromol. Rapid Commun.* **31**, 150–68 (2010).
 - [9] Knorowski, C. & Travesset, A. Materials design by DNA programmed self-assembly. *Curr. Opin. Solid State Mater. Sci.* **15**, 262–270 (2011).
 - [10] Geerts, N. & Eiser, E. DNA-functionalized colloids: Physical properties and applications. *Soft Matter* **6**, 4647 (2010).
 - [11] Di Michele, L. & Eiser, E. Developments in understanding and controlling self assembly of DNA-functionalized colloids. *Phys. Chem. Chem. Phys.* **15**, 3115–29 (2013).
 - [12] Manoharan, V. N., Elsesser, M. T. & Pine, D. J. Dense packing and symmetry in small clusters of microspheres. *Science (New York, N.Y.)* **301**, 483–7 (2003).
 - [13] Licata, N. & Tkachenko, A. Self-assembly of DNA-coded nanoclusters. *Phys. Rev. E* **74**, 040401 (2006).

- [14] Licata, N. & Tkachenko, A. V. How to build nanoblocks using DNA scaffolds. *Europhys. Lett.* **84**, 20010 (2008).
- [15] Soto, C. M., Srinivasan, A. & Ratna, B. R. Controlled assembly of mesoscale structures using DNA as molecular bridges. *J. Am. Chem. Soc.* **124**, 8508–9 (2002).
- [16] Fan, J. A. *et al.* DNA-enabled self-assembly of plasmonic nanoclusters. *Nano Lett.* **11**, 4859–64 (2011).
- [17] Hormoz, S. & Brenner, M. P. Design principles for self-assembly with short-range interactions. *PNAS* **108**, 5193–8 (2011).
- [18] Hagan, M. F. & Chandler, D. Dynamic pathways for viral capsid assembly. *Biophys. J.* **91**, 42–54 (2006).
- [19] Jack, R., Hagan, M. & Chandler, D. Fluctuation-dissipation ratios in the dynamics of self-assembly. *Phys. Rev. E* **76**, 021119 (2007).
- [20] Grant, J., Jack, R. L. & Whitlam, S. Analyzing mechanisms and microscopic reversibility of self-assembly. *J. Chem. Phys.* **135**, 214505 (2011).
- [21] Henzie, J., Grünwald, M., Widmer-Cooper, A., Geissler, P. L. & Yang, P. Self-assembly of uniform polyhedral silver nanocrystals into densest packings and exotic superlattices. *Nature Materials* **11**, 131–7 (2012).
- [22] Miszta, K. *et al.* Hierarchical self-assembly of suspended branched colloidal nanocrystals into superlattice structures. *Nature Materials* **10**, 872–6 (2011).
- [23] Damasceno, P. F., Engel, M. & Glotzer, S. C. Predictive self-assembly of polyhedra into complex structures. *Science* **337**, 453–7 (2012).
- [24] Fletcher, D. A. & Mullins, R. D. Cell mechanics and the cytoskeleton. *Nature* **463**, 485–92 (2010).
- [25] Anderson, J. A., Lorenz, C. D. & Travesset, A. General purpose molecular dynamics simulations fully implemented on graphics processing units. *J. Comput. Phys.* **227**, 5342–5359 (2008).
- [26] Nguyen, T. D., Phillips, C. L., Anderson, J. A. & Glotzer, S. C. Rigid body constraints realized in massively-parallel molecular dynamics on graphics processing units. *Comp. Phys. Commun.* **182**, 2307–2313 (2011).
- [27] Humphrey, W., Dalke, A. & Schulten, K. VMD: visual molecular dynamics. *J. Mol. Graphics* **14**, 33–8 (1996).
- [28] We consider only attractive interactions with $\epsilon_{AB} \geq 0$. Negative values of ϵ effectively increase the size of monomers. Because of the short range of interactions, this modification is subtle and has little effect on assembly dynamics.